FEBS Letters 589 (2015) 1406–1411

FEBS Letters

journal homepage: www.FEBSLetters.org

Biselyngbyasides, cytotoxic marine macrolides, are novel and potent inhibitors of the Ca^{2+} pumps with a unique mode of binding

Maho Morita [a,b], Haruo Ogawa [b], Osamu Ohno [a], Takao Yamori [c], Kiyotake Suenaga [a], Chikashi Toyoshima [b,*]

[a] Department of Chemistry, Keio University, Kohoku-ku, Yokohama, Kanagawa 223-8522, Japan
[b] Institute of Molecular and Cellular Biosciences, The University of Tokyo, Bunkyo-ku, Tokyo 113-0032, Japan
[c] Cancer Chemotherapy Center, Japanese Foundation for Cancer Research, Ariake, Koto-ku, Tokyo 135-8550, Japan

ARTICLE INFO

Article history:
Received 31 March 2015
Revised 24 April 2015
Accepted 27 April 2015
Available online 6 May 2015

Edited by Peter Brzezinski

Keywords:
Crystal structure
Ca^{2+}-ATPase
Ion pump
Inhibitor
High affinity
Macrolide

ABSTRACT

Biselyngbyasides (BLSs), macrolides from a marine cyanobacterium, are cytotoxic natural products whose target molecule is unknown. Here we report that BLSs are high affinity ($K_i \sim 10$ nM) inhibitors of Ca^{2+}-pumps with a unique binding mode. The crystal structures of the Ca^{2+}-pump in complex with BLSs at 3.2–3.5 Å-resolution show that BLSs bind to the pump near the cytoplasmic surface of the transmembrane region. The crystal structures and activity measurement of BLS analogs allow us to identify the structural features that confer high potency to BLSs as inhibitors of the pump.

1. Introduction

Natural products and their derivatives are rich sources of pharmaceutical lead compounds for the treatment of various diseases [1–3]. Especially in the area of cancer chemotherapy, more than half of anticancer agents are derived from or inspired by natural products [4]. Biselyngbyasides (BLSs, **1**–**4**, Fig. 1) are macrolides that display potent cytotoxicity against a variety of human cancer cells (e.g. GI_{50} of **1** = 36 nM for the central nervous system cancer cells SNB-78, 67 nM for lung cancer cells NCI H522) [5–8]. To date, six BLSs have been isolated from the marine cyanobacterium *Lyngbya* sp. The best studied is biselyngbyaside [5] (BLS, **1**), featuring a glycosylated 18-membered macrolactone containing a conjugated 1,3-diene, two olefins, and a side chain at C17. We previously showed that BLS (**1**) inhibits osteoclastgenesis and induces apoptosis of osteoclasts [9], and that the cytotoxicities of BLS analogs vary dramatically depending on their structures [6] (e.g. IC_{50} against HeLa cells: 2.5 μM for **1**, 0.0028 μM for **2**, 0.0039 μM for **3**, >10 μM for **4**). It is unknown why the cyanobacterium produces BLSs. In general, however, toxic secondary metabolites are hypothesized to protect cyanobacteria from predator such as mollusk and crustacean, or provide a competitive advantage for survival over other microorganisms.

To predict the target protein of BLSs, BLS (**1**) was submitted to Japanese Foundation for Cancer Research 39 (JFCR39) anticancer drug screening system (Table 1) [5]. The inhibition profile was similar to that of thapsigargin [10] (TG, **5**, Fig. 1), a potent inhibitor of sarco/endoplasmic reticulum (SR/ER) Ca^{2+}-ATPases (SERCA) [11], the calcium pump responsible for establishing the Ca^{2+} concentration gradient across the SR/ER membrane. The inhibition profile of BLS is also similar, though not to the same extent, to those of cyclopiazonic acid (CPA, **6**) [12–15] and 2,5-di-*tert*-butyl-1, 4-benzohydroquinone (BHQ, **7**) [16,17], known inhibitors of SERCA. However, BLSs have no structural resemblance to any of

Abbreviations: BHC, benzene hexachloride; BHQ, 2,5-di-*tert*-butyl-1, 4-benzohydroquinone; BLLA, biselyngbyolide A; BLLB, biselyngbyolide B; BLS, biselyngbyaside; BLSC, baselyngbyaside C; $C_{12}E_8$, octaethyleneglycol-*n*-dodecylether; CPA, cyclopiazonic acid; JFCR39, Japanese Foundation for Cancer Research 39; PC, phosphatidylcholine; PE, phosphatidylethanolamine; SERCA, sarco/endoplasmic reticulum (SR/ER) Ca^{2+}-ATPases; SR, sarcoplasmic reticulum; TG, thapsigargin

Author contributions: C.T. supervised the study; M.M., C.T., O.O. and K.S. conceived the study; M.M., C.T. and H.O. performed experiments; C.T. and H.O. supervised structure refinement; M.M. and H.O. analyzed data; T.Y. analyzed the data from JFCR39 screening system; M.M. and C.T. wrote the manuscript.

* Corresponding author.
E-mail address: ct@iam.u-tokyo.ac.jp (C. Toyoshima).

http://dx.doi.org/10.1016/j.febslet.2015.04.056
0014-5793/

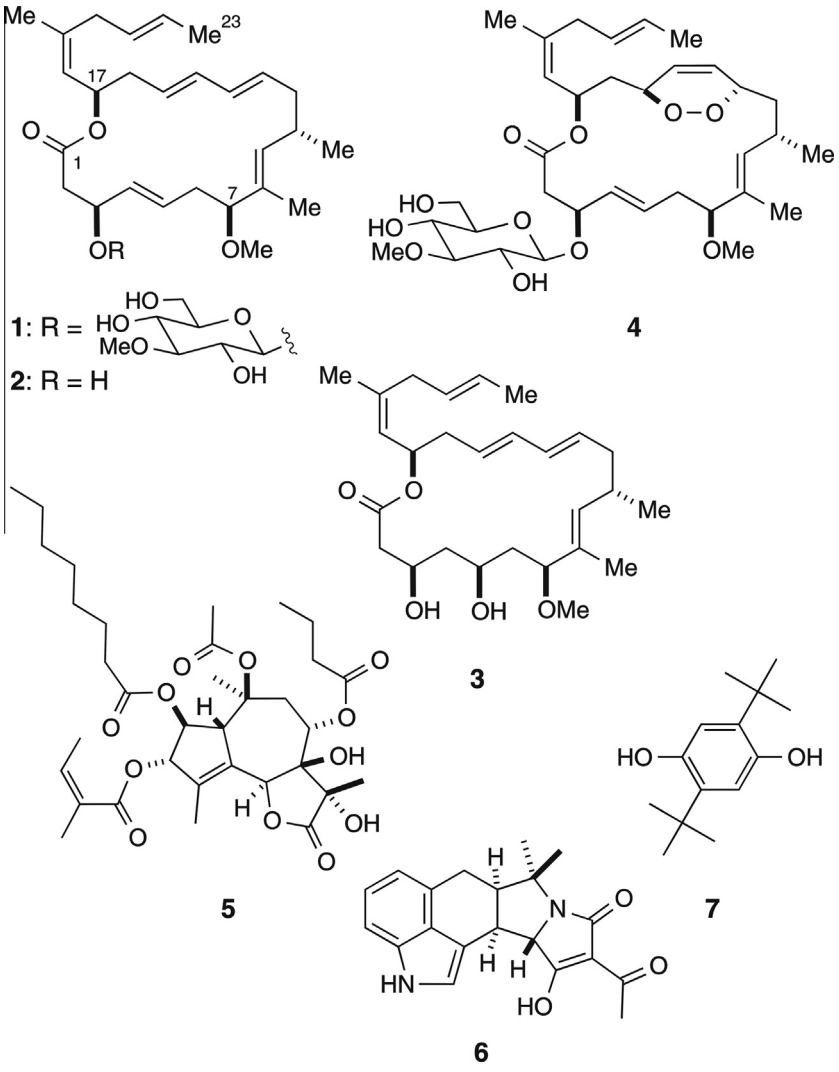

Fig. 1. Structures of biselyngbyasides and inhibitors of SERCA.

Table 1
Correlation between growth inhibition profiles of BLS and reference chemicals.

Rank	*r* value[a]	Reference chemical	Function
1	0.706[b,c]	TG	SERCA inhibitor
2	0.653[c]	Pyriproxyfen	Insecticide
3	0.622[b,c]	TG	SERCA inhibitor
4	0.590	γ-BHC[d]	Insecticide
5	0.589	CPA	SERCA inhibitor
6	0.571	Methoprene	Juvenile hormone analog
7	0.565	Dieldrin	Insecticide
8	0.559	BHQ	SERCA inhibitor
:	:		
:	:		

[a] Pearson correlation coefficient between the 50% growth inhibition (GI_{50}) profile of BLS and that of the reference chemical.
[b] Two values were obtained by independent tests.
[c] It is generally accepted that an *r* value of >0.6 suggests a mode of action similar to that of the reference chemical.
[d] γ-Benzene hexachloride.

them. Since inhibition of SERCA results in activation of ER-stress response and induction of apoptotic cell death [18,19], SERCA inhibitors are now of great interest as lead compounds for cancer chemotherapy [20,21]. For instance, a peptide-conjugated derivative of TG has been in human phase II evaluation as a chemotherapeutic agent against prostate cancer [20].

The SERCA family consists of SERCA1–3 [22,23], of which the best-studied member is SERCA1a, which is abundant in fast-twitch skeletal muscle. SERCA1a is composed of a large cytoplasmic headpiece consisting of A (actuator), N (nucleotide binding) and P (phosphorylation) domains, and 10 transmembrane helices (M1–M10) [24,25]. According to classical E1/E2 theory [26,27], in which SERCA1a has high affinity for Ca^{2+} in E1 but low affinity in E2, active transport of Ca^{2+} is achieved by alternating the affinity for Ca^{2+} and the sidedness of the binding sites [28].

2. Results and discussion

We evaluated the effect of BLSs (**1**–**4**) on the ATPase activity of SERCA1a and 2a by a coupled enzyme assay (Supplementary Fig. S2). BLSs (**1**–**3**) strongly inhibited SERCA1a (K_i = 19 nM for **1**, 17 nM for **2**, ~9 nM for **3**) similar to TG (**5**), whereas biselyngbyaside C (BLSC, **4**) was only weakly active (K_i = 18 μM) (Table 2). The low affinity of BLSC (**4**) to SERCA is consistent with the cell-based assessment of BLSs [6], but the comparable affinity of BLS (**1**) to those of biselyngbyolide B (BLLB, **2**) and biselyngbyolide A (BLLA, **3**) is markedly different.

Table 2
Activities of SERCA inhibitors.

No. compound		K_i (nM)	
		SERCA1a[a]	SERCA2a
1	BLS	19	11
2	BLLB	17	27
3	BLLA	(9)[b]	–
4	BLSC	18,000	1300
5	TG	*0.1* (Ref. [11])	–
6	CPA	1800	–
7	BHQ	*400* (Ref. [16])	–

[a] Published data are shown in italics.
[b] Preliminary data.

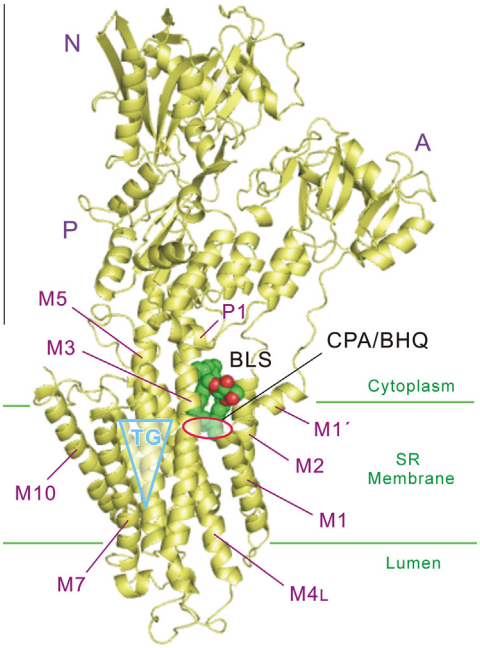

Fig. 2. Crystal structure of SERCA1a with bound biselyngbyaside. Structure of E2(BLS) in a ribbon representation. Biselyngbyaside (BLS; green and red) is shown as spheres. The binding sites of thapsigargin (TG, cyan triangle), cyclopiazonic acid (CPA; red circle) and 2,5-di-*tert*-butyl-1,4-benzohydroquinone (BHQ) are indicated.

Crystals of SERCA1a in complex with BLSs were grown under E2 conditions in the absence of Ca^{2+} but in the presence of BLS or BLLB, and diffracted to ~3.0 Å resolution. Structures were solved by molecular replacement using the crystal structure of SERCA1a in E2 with bound CPA [abbreviated as E2(CPA), Protein Data Bank (PDB) ID 4YCL [14]] as the starting model. The $|F_{obs}| - |F_{calc}|$ electron density maps of E2(BLS) and E2(BLLB), before introducing BLS/BLLB into the atomic models, unambiguously identified BLS/BLLB near the cytoplasmic surface of the transmembrane region (Fig. 2). Additionally, the Fourier difference ($|F_{obs}|_{BLS} - |F_{obs}|_{BLLB}$) map allowed us to assign the position of the sugar moiety of BLS (Supplementary Fig. S3) and the atomic models were refined to R_{free} of 26.0% at 3.2 Å [E2(BLS)] (PDB ID: 4YCM) and 24.7% at 3.5 Å [E2(BLLB)] (PDB ID: 4YCN) (Supplementary Table S1). The binding details of BLSs were examined using the $|F_{obs}| - |F_{calc}|$ omit annealed electron density maps (Supplementary Fig. S4).

In the structures of E2(BLS) and E2(BLLB), the transmembrane helices M1–M4 and the P domain helix P1 contribute to form the binding sites of BLS/BLLB (Fig. 3a–c and Supplementary Fig. S5). The two crystal structures are superimposable (root mean squared deviation (r.m.s.d.) 0.22 Å) including BLS and BLLB themselves, and the residues interacting with BLSs are basically the same (Fig. 3a and b).

The C10–C17 segment of BLS/BLLB occupies the cleft between the M3 and M4 helices forming van der Waals contacts with hydrophobic residues (Fig. 3a–c). Of particular interest are the 1,3-diene moiety at C12 and the side chain at C17. The 1,3-diene moiety in the lactone ring contacts Leu253 on M3, and Leu311, Pro312, and Ile315 on M4. The hydrophobicity, compactness, and linearity of the conjugated diene allow such interactions. The crystal structure of E2(BLS) readily explains the distinctively low affinity of BLSC, as the 1,3-diene of BLS is substituted by a bulky endoperoxide moiety. The C18–C23 side chain is located in the cytoplasmic region of SERCA1a protruding into a narrow space surrounded by M3, M4, and P1 helices (Fig. 3c). The aperture is too small to allow elaboration around the vinyl methyl group at C19, and the geometry of the olefin at C18 must be important in gaining a high affinity.

The hydrophilic substituents on the other side of the lactone ring also contribute to binding by forming hydrogen bonds. For instance, the methoxy oxygen at C7 likely forms a hydrogen bond with Asn101 on M2. The hydroxyl group at C3 of BLLB could form another hydrogen bond with Gln56 on M1′. When the sugar moiety is present as in BLS, further hydrogen bonds with Asp59 and Asp254 are likely. In contrast to the narrow space in the cleft between M3 and M4, there is a large empty space around the C2–C6 part of the lactone ring. Indeed, BLLA (**3**) with a hydroxyl group at C5 retains a similar inhibitory activity against SERCA1a as BLLB (**2**) (Table 2, Supplementary Fig. S2).

The crystal structures show that the binding site of the BLSs is well separated from that of TG (cyan triangle in Fig. 2), but partially overlaps with those of CPA and BHQ (red circle in Fig. 2). Like the BLSs, CPA forms hydrogen bonds with the side chains of Gln56, Asp59, and Asn101, but there are far less hydrophobic contacts with residues on M3, M4, and P1, explaining the high affinity of BLSs compared with that of CPA (Fig. 4).

A comparison of the E2 (PDB ID: 3W5D [30]) and E2(BLLB) crystal structures gives a clear picture of the conformational change of SERCA1a on binding BLLB (Fig. 5). Whereas the M3 and M4 helices occupy almost the same positions (r.m.s.d. 0.22 Å), binding of BLLB pushes M1 toward M3 through Leu61 (dotted circle in Fig. 5), thereby pulling M1′, a short amphipathic helix linked to M1, toward BLLB. As a result, the side chain of Gln56 comes within hydrogen bonding distance of the hydroxyl group at C3 of BLLB. As the M1–M2 V-shaped structure moves as a rigid body [24], M2 inclines by 8° toward BLLB, causing Asn101 to hydrogen bond with the methoxy oxygen at C7 and Gly105 to contact (3.3 Å) the carbonyl oxygen at C1 of BLLB. Thus, Asn101 stabilizes the position of the M2 helix and tightens the binding pocket. The binding of BLSs would cause a steric clash with a phospholipid molecule (modeled as phosphatidylethanolamine (PE) [17] in Fig. 5) located between the M2 and M4 helices in E2. Indeed the electron density maps of both E2(BLS) and E2(BLLB) are devoid of density corresponding to this phospholipid molecule, as in that of E2(CPA) [14].

As described earlier, the BLSs bind to SERCA1a in the Ca^{2+}-free E2 state. To examine whether BLS/BLLB can bind to a Ca^{2+}-bound state, we superimposed the atomic models of E2(BLLB) and E1·2Ca^{2+} (PDB ID: 1SU4 [25]; Fig. 6). Due to the large-scale rearrangement of M1–M6 helices in the transition from E2(BLLB) to E1·2Ca^{2+}, a steric clash between M1 (e.g. Trp50) and BLS/BLLB is inevitable if BLS/BLLB moves together with the M3–M4 helices (Fig. 6 inset), making BLS/BLLB binding impossible in E1·2Ca^{2+}.

In summary, we have determined the crystal structures of SERCA1a in complex with BLS and BLLB, and find that the macrolides exhibit extensive hydrophobic contacts with transmembrane helices M3 and M4, and the cytoplasmic P1 helix in addition to several hydrogen bonds. The BLSs strongly inhibit ATPase activities of SERCA1a and 2a, and the crystal structures suggest that the 1,3-diene moiety and the side chain of BLS/BLLB play important

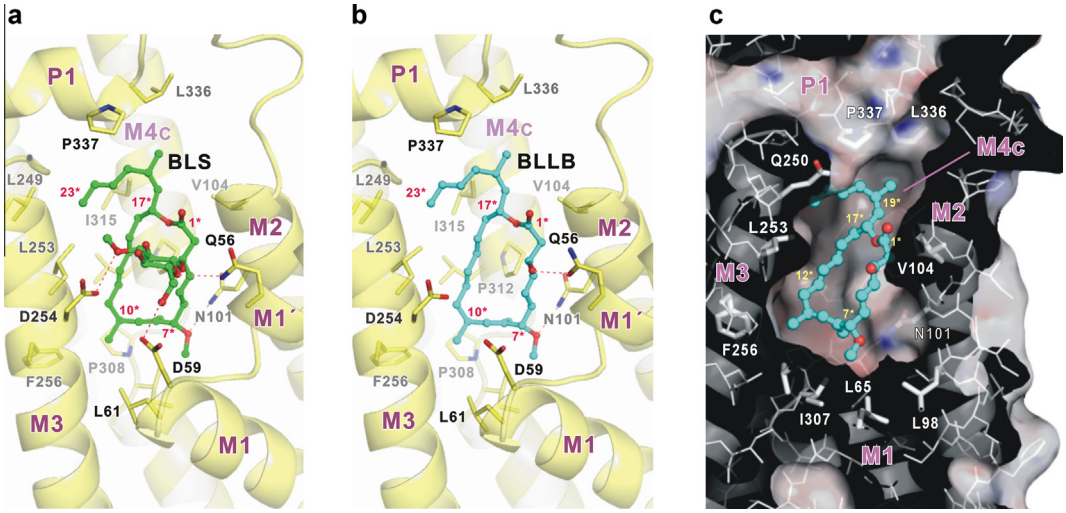

Fig. 3. Crystal structures of SERCA1a with bound biselyngbyasides. (a and b) The binding sites of BLS (a; green and red) and biselyngbyolide B (b; BLLB, cyan and red). Side chains interacting with BLS or BLLB are shown in yellow stick. (c) A cross-section of the SERCA1a-BLLB complex around the BLLB-binding site, viewed approximately parallel to the membrane. Surface color changes according to the surface potential: red, negative; blue, positive. Gray ribbons identify the transmembrane helices.

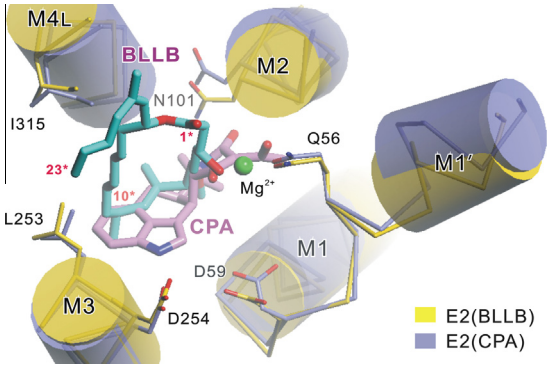

Fig. 4. Superimposition of E2(BLLB) and E2(CPA). Yellow, E2(BLLB); blue gray, E2(CPA) (PDB ID: 4YCL). Cylinders represent transmembrane helices. Viewed from the cytoplasmic side approximately perpendicular to the membrane. A Mg^{2+} ion is found only in E2(CPA) [29].

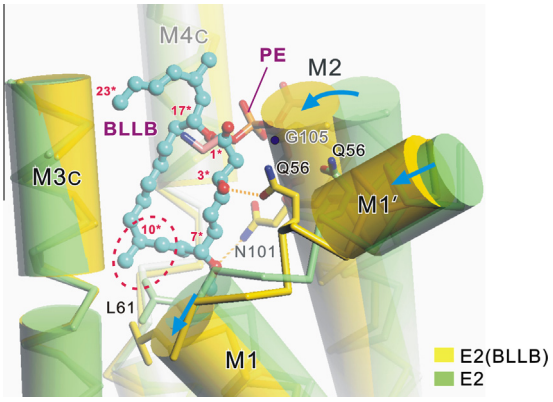

Fig. 5. Superimposition of E2(BLLB) and E2 (PDB ID: 3W5D). Cylinders represent transmembrane helices. Yellow, E2(BLLB); light green, E2. PE refers to the phospholipid head group of phosphatidylethanolamine identified in only the E2 crystal structure [30]. Arrows show the movements from E2 to E2(BLLB). The Dotted circle marks the atoms expected to push Leu61 in E2.

roles in the high affinities and unique binding mode. The structures will facilitate rational design of chemical probes for studies of SERCA as well as the development of drugs for treating SERCA-related diseases.

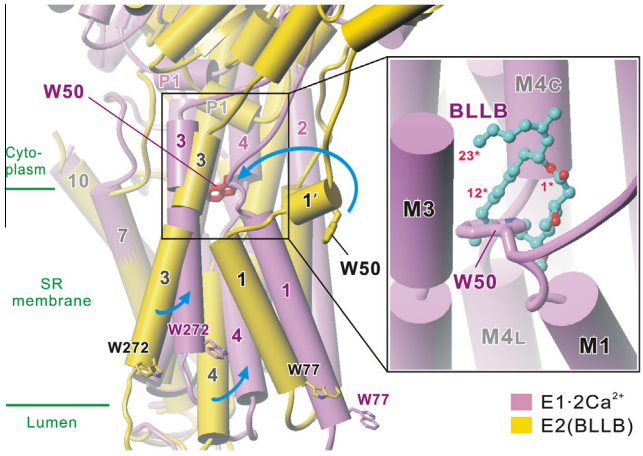

Fig. 6. Superimposition of E2(BLLB) and E1·2Ca^{2+}. SERCA1a are shown in a cylinder. Yellow, E2(BLLB); magenta, E1·2Ca^{2+}. Viewed approximately parallel to the membrane. Arrows show the movements from E2(BLLB) to E1·2Ca^{2+}. The inset illustrates steric clash expected to occur between BLLB and SERCA1a in E1·2Ca^{2+}.

3. Materials and methods

3.1. Isolation of biselyngbyasides

BLSs were isolated from the marine cyanobacterium *Lyngbya* sp., as described previously [5–8]. Briefly, methanol extract of *Lyngbya* sp. was partitioned between ethyl acetate and water, and then 90% aqueous methanol and hexane. The 90% aqueous methanol fraction was fractionated by ODS silica gel column and then subjected to reversed-phase HPLC chromatography to give BLSs (**1**–**4**).

3.2. Biochemical procedures

Sarcoplasmic reticulum (SR) vesicles were obtained from white skeletal muscle of rabbit hind legs as described by Eletr and Inesi [31] and solubilized with 2% octaethyleneglycol-*n*-dodecylether ($C_{12}E_8$). Dye affinity chromatography was used for purifying SERCA1a as described [32]. For the microsome containing wild-type SERCA2a, COS cells infected with recombinant adenovirus were cultured and collected following the protocol

developed for SERCA1a [30]. The microsomal fraction of the virus-infected cells was purified as reported previously [33]. SR vesicles (SERCA1a) and microsomes (SERCA2a) were used for measuring ATPase activity by coupled enzyme assay [34]. ATP hydrolysis by hexokinase was examined in the presence of BLS to confirm that BLS has no effect on the assay system.

3.3. Crystallization

Crystals of E2(BLS) were obtained by dialysis and those of E2(BLLB) by vapor diffusion, both at 10 °C. The crystallization conditions were essentially the same as those reported previously for E2(TG) [35]. For the crystal of E2(BLS), the protein solution containing 2 mg ml^{-1} affinity-purified SERCA1a, 0.17% $C_{12}E_8$, 0.7 mg ml^{-1} phosphatidylcholine (PC), 1 mM $MgCl_2$, 16% glycerol, 0.2 mM BLS, and 3 mM *O,O′*-bis(2-aminoethyl) ethyleneglycol-*N,N,N′,N′*-tetraacetic acid (EGTA) was dialyzed against a buffer consisting of 25% glycerol, 9% PEG2000, 1 mM $MgCl_2$, 25 mM $MgSO_4$, 2.5 mM NaN_3, 2 mg ml^{-1} butylhydroxytoluene (BHT), 0.2 mM dithiothreitol (DTT), 1 mM EGTA, and 20 mM MES, pH 6.1, for 2 weeks. For the crystals of E2(BLLB), the protein solution contained 4 mg ml^{-1} affinity-purified SERCA1a, 0.07% $C_{12}E_8$, 0.5 mg ml^{-1} PC, 1 mM $MgCl_2$, 18% glycerol, 0.05 mM BLLB, and 2 mM EGTA, 10 mM MOPS, 10 mM MES, pH 6.1. The reservoir consisted of 16% glycerol, 14% PEG3350, 1 mM $MgCl_2$, 200 mM $MgSO_4$, 1 mM EGTA, pH 6.1. One microliter each of the protein and the reservoir solutions were mixed, and the crystals grew in 2 weeks. The crystals were flash frozen in cold nitrogen gas and stored in liquid nitrogen until use.

3.4. Data collection and structure determination

Diffraction data were collected at BL41XU of Spring-8 with a Pilatus3 6 M detector. Denzo and Scalepack [36] were used to process diffraction data. For the structure of E2(BLLB), diffraction intensities from the two best crystals were merged. Unit cell parameters and data statistics are listed in Table S1. The atomic models were built by molecular replacement with MOLREP [37] using the re-refined atomic model for E2(CPA) [PDB ID: 4YCL [14]] as the starting model, and refined with CNS [38] and PHENIX [39]. The geometry of the models was examined with ProCheck [40]. Structural figures were prepared with TurboFRODO and Pymol (http://www.pymol.org/).

Acknowledgments

We thank K. Hasegawa and H. Okumura of the Japan Synchrotron Radiation Research Institute (JASRI) for data collection at BL41XU of SPring-8 and J. Tsueda for preparing purified enzyme. We are grateful to D.B. McIntosh for help in improving the manuscript. This work was supported by a Specially Promoted Project Grant (23000014 to C.T.) and Grants-in-Aid (241310160 to K.S. and 13J00542 to M.M.) from Ministry of Education, Culture, Sports, Science, and Technology of Japan.

Appendix A. Supplementary data

Supplementary data associated with this article can be found, in the online version, at http://dx.doi.org/10.1016/j.febslet.2015.04.056.

References

[1] Molinski, T.F., Dalisay, D.S., Lievens, S.L. and Saludes, J.P. (2009) Drug development from marine natural products. Nat. Rev. Drug Discovery 8, 69–85.
[2] Butler, M.S., Robertson, A.A.B. and Cooper, M.A. (2014) Natural product and natural product derived drugs in clinical trials. Nat. Prod. Rep. 31, 1612–1661.
[3] Szychowski, J., Truchon, J.-F. and Bennani, Y.L. (2014) Natural products in medicine: transformational outcome of synthetic chemistry. J. Med. Chem. 57, 9292–9308.
[4] Cragg, G.M., Grothaus, P.G. and Newman, D.J. (2009) Impact of natural products on developing new anti-cancer agents. Chem. Rev. 109, 3012–3043.
[5] Teruya, T., Sasaki, H., Kitamura, K., Nakayama, T. and Suenaga, K. (2009) Biselyngbyaside, a macrolide glycoside from the marine cyanobacterium *Lyngbya* sp. Org. Lett. 11, 2421–2424.
[6] Morita, M., Ohno, O., Teruya, T., Yamori, T., Inuzuka, T. and Suenaga, K. (2012) Isolation and structures of biselyngbyasides B, C, and D from the marine cyanobacterium *Lyngbya* sp., and the biological activities of biselyngbyasides. Tetrahedron 68, 5984–5990.
[7] Morita, M., Ohno, O. and Suenaga, K. (2012) Biselyngbyolide A, a novel cytotoxic macrolide from the marine cyanobacterium *Lyngbya* sp. Chem. Lett. 41, 165–167.
[8] Ohno, O., Watanabe, A., Morita, M. and Suenaga, K. (2014) Biselyngbyolide B, a novel ER stress-inducer isolated from the marine cyanobacterium *Lyngbya* sp. Chem. Lett. 43, 287–289.
[9] Yonezawa, T., Mase, N., Sasaki, H., Teruya, T., Hasegawa, S., Cha, B.Y., Yagasaki, K., Suenaga, K., Nagai, K. and Woo, J.T. (2012) Biselyngbyaside, isolated from marine cyanobacteria, inhibits osteoclastogenesis and induces apoptosis in mature osteoclasts. J. Cell. Biochem. 113, 440–448.
[10] Christensen, S.B., Larsen, I.K., Rasmussen, U. and Christophersen, C. (1982) Thapsigargin and thapsigargicin, two histamine liberating sesquiterpene lactones from *Thapsia garganica*. X-ray analysis of the 7,11-epoxide of thapsigargin. J. Org. Chem. 47, 649–652.
[11] Sagara, Y. and Inesi, G. (1991) Inhibition of the sarcoplasmic reticulum Ca^{2+} transport ATPase by thapsigargin at subnanomolar concentrations. J. Biol. Chem. 266, 13503–13506.
[12] Goeger, D.E., Riley, R.T., Dorner, J.W. and Cole, R.J. (1988) Cyclopiazonic acid inhibition of the Ca^{2+}-transport ATPase in rat skeletal muscle sarcoplasmic reticulum vesicles. Biochem. Pharmacol. 37, 978–981.
[13] Seidler, N.W., Jona, I., Vegh, M. and Martonosi, A. (1989) Cyclopiazonic acid is a specific inhibitor of the Ca^{2+}-ATPase of sarcoplasmic reticulum. J. Biol. Chem. 264, 17816–17823.
[14] Takahashi, M., Kondou, Y. and Toyoshima, C. (2007) Interdomain communication in calcium pump as revealed in the crystal structures with transmembrane inhibitors. Proc. Natl. Acad. Sci. USA 104, 5800–5805.
[15] Moncoq, K., Trieber, C.A. and Young, H.S. (2007) The molecular basis for cyclopiazonic acid inhibition of the sarcoplasmic reticulum calcium pump. J. Biol. Chem. 282, 9748–9757.
[16] Khan, Y.M., Wictome, M., East, J.M. and Lee, A.G. (1995) Interactions of dihydroxybenzenes with the Ca^{2+}-ATPase: separate binding sites for dihydroxybenzenes and sesquiterpene lactones. Biochemistry 34, 14385–14393.
[17] Obara, K., Miyashita, N., Xu, C., Toyoshima, I., Sugita, Y., Inesi, G. and Toyoshima, C. (2005) Structural role of countertransport revealed in Ca^{2+} pump crystal structure in the absence of Ca^{2+}. Proc. Natl. Acad. Sci. USA 102, 14489–14496.
[18] Liu, H., Bowes 3rd, R.C., van de Water, B., Sillence, C., Nagelkerke, J.F. and Stevens, J.L. (1997) Endoplasmic reticulum chaperones GRP78 and calreticulin prevent oxidative stress, Ca^{2+} disturbances, and cell death in renal epithelial cells. J. Biol. Chem. 272, 21751–21759.
[19] Caspersen, C., Pedersen, P.S. and Treiman, M. (2000) The sarco/endoplasmic reticulum calcium-ATPase 2b is an endoplasmic reticulum stress-inducible protein. J. Biol. Chem. 275, 22363–22372.
[20] Doan, N.T., Paulsen, E.S., Sehgal, P., Møller, J.V., Nissen, P., Denmeade, S.R., Isaacs, J.T., Dionne, C.A. and Christensen, S.B. (2015) Targeting thapsigargin towards tumors. Steroids 97, 2–7.
[21] Dubois, C., Vanden Abeele, F., Sehgal, P., Olesen, C., Junker, S., Christensen, S.B., Prevarskaya, N. and Møller, J.V. (2013) Differential effects of thapsigargin analogues on apoptosis of prostate cancer cells: complex regulation by intracellular calcium. FEBS J. 280, 5430–5440.
[22] Lytton, J., Westlin, M., Burk, S.E., Shull, G.E. and MacLennan, D.H. (1992) Functional comparisons between isoforms of the sarcoplasmic or endoplasmic reticulum family of calcium pumps. J. Biol. Chem. 267, 14483–14489.
[23] Burk, S.E., Lytton, J., MacLennan, D.H. and Shull, G.E. (1989) CDNA cloning, functional expression, and mRNA tissue distribution of a third organellar Ca^{2+} pump. J. Biol. Chem. 264, 18561–18568.
[24] Toyoshima, C. (2008) Structural aspects of ion pumping by Ca^{2+}-ATPase of sarcoplasmic reticulum. Arch. Biochem. Biophys. 476, 3–11.
[25] Toyoshima, C., Nakasako, M., Nomura, H. and Ogawa, H. (2000) Crystal structure of the calcium pump of sarcoplasmic reticulum at 2.6 Å resolution. Nature 405, 647–655.
[26] Albers, R.W. (1967) Biochemical aspects of active transport. Annu. Rev. Biochem. 36, 727–756.
[27] Post, R.L., Hegyvary, C. and Kume, S. (1972) Activation by adenosine triphosphate in the phosphorylation kinetics of sodium and potassium ion transport sdenosine triphosphatase. J. Biol. Chem. 247, 6530–6540.
[28] de Meis, L. and Vianna, A.L. (1979) Energy interconversion by the Ca^{2+}-dependent ATPase of the sarcoplasmic reticulum. Annu. Rev. Biochem. 48, 275–292.
[29] Laursen, M., Bublitz, M., Moncoq, K., Olesen, C., Møller, J.V., Young, H.S., Nissen, P. and Morth, J.P. (2009) Cyclopiazonic acid is complexed to a divalent metal

ion when bound to the sarcoplasmic reticulum Ca^{2+}-ATPase. J. Biol. Chem. 284, 13513–13518.
[30] Toyoshima, C., Iwasawa, S., Ogawa, H., Hirata, A., Tsueda, J. and Inesi, G. (2013) Crystal structures of the calcium pump and sarcolipin in the Mg^{2+}-bound E1 state. Nature 495, 260–264.
[31] Eletr, S. and Inesi, G. (1972) Phospholipid orientation in sarcoplasmic membranes: spin-label ESR and proton MNR studies. Biochim. Biophys. Acta 282, 174–179.
[32] Coll, R.J. and Murphy, A.J. (1984) Purification of the CaATPase of sarcoplasmic reticulum by affinity chromatography. J. Biol. Chem. 259, 14249–14254.
[33] Autry, J.M. and Jones, L.R. (1997) Functional co-expression of the canine cardiac Ca^{2+} pump and phospholamban in *Spodoptera frugiperda* (Sf21) cells reveals new insights on ATPase regulation. J. Biol. Chem. 272, 15872–15880.
[34] Warren, G.B., Toon, P.A., Birdsall, N.J., Lee, A.G. and Metcalfe, J.C. (1974) Reconstitution of a calcium pump using defined membrane components. Proc. Natl. Acad. Sci. USA 71, 622–625.
[35] Toyoshima, C. and Nomura, H. (2002) Structural changes in the calcium pump accompanying the dissociation of calcium. Nature 418, 605–611.
[36] Otwinowski, Z. and Minor, W. (1997) Processing of X-ray diffraction data collected in oscillation mode. Methods Enzymol. 276, 307–326.
[37] Vagin, A. and Teplyakov, A. (1997) MOLREP: an automated program for molecular replacement. J. Appl. Crystallogr. 30, 1022–1025.
[38] Brünger, A.T., Adams, P.D., Clore, G.M., DeLano, W.L., Gros, P., Grosse-Kunstleve, R.W., Jiang, J.S., Kuszewski, J., Nilges, M., Pannu, N.S., Read, R.J., Rice, L.M., Simonson, T. and Warren, G.L. (1998) Crystallography & NMR system: a new software suite for macromolecular structure determination. Acta Crystallogr. D Biol. Crystallogr. 54, 905–921.
[39] Adams, P.D., Afonine, P.V., Bunkoczi, G., Chen, V.B., Davis, I.W., Echols, N., Headd, J.J., Hung, L.W., Kapral, G.J., Grosse-Kunstleve, R.W., McCoy, A.J., Moriarty, N.W., Oeffner, R., Read, R.J., Richardson, D.C., Richardson, J.S., Terwilliger, T.C. and Zwart, P.H. (2010) PHENIX: a comprehensive Python-based system for macromolecular structure solution. Acta Crystallogr. D Biol. Crystallogr. 66, 213–221.
[40] Collaborative Computational project, Number 4 (1994) The CCP4 suite: programs for protein crystallography. Acta Crystallogr. D Biol. Crystallogr. 50, 760–763.